CRYSTAL GROWTH & DESIGN

Article

pubs.acs.org/crystal

Syntheses, Structures, and Magnetic Properties of Three Manganese(II)-Octacyanotungstate(V) Bimetallic Compounds with Linear Ligands

Fei-Lin Yang,[†] Ai-Hua Yuan,*[,†] Hu Zhou,[‡] Hong-Bo Zhou,[§] Dan Yang,[†] You Song,*[,#] and Yi-Zhi Li[#]

[†]School of Environmental and Chemical Engineering, and [‡]School of Material Science and Engineering, Jiangsu University of Science and Technology, Zhenjiang 212003, P. R. China

[§]School of Chemistry and Chemical Engineering, Jiangsu University, Zhenjiang 212013, P. R. China

[#]State Key Laboratory of Coordination Chemistry, Nanjing National Laboratory of Microstructures, School of Chemistry and Chemical Engineering, Nanjing University, Nanjing 210093, P. R. China

Supporting Information

ABSTRACT: Three manganese(II)-octacyanotungstate(V) bimetallic compounds, $[Mn(H_2O)_2(dpe)]_3[W(CN)_8]_2\cdot 2dpe\cdot 7H_2O$ (dpe = *trans*-1,2-di(4-pyridyl)ethene) (**1**), $[Mn(H_2O)_2(azpy)]_3[W(CN)_8]_2\cdot 3azpy\cdot 4H_2O$ (azpy = 4,4′-azopyridine) (**2**), and $[Mn(H_2O)_3(azpy)]_2[Mn(CH_3CN)_2(azpy)][W(CN)_8]_2\cdot 5azpy\cdot 2H_2O$ (**3**) were prepared by in situ or secondary assembly methods. Compounds **1** and **2** show three-dimensional (3D) networks through the cross-link of one-dimensional (1D) infinite 3,2-chains or rope-ladder chains with linear ligands (dpe, azpy), while compound **3** adopts a 1D ribbon-like structure by the connection of pentanuclear repeating units with azpy linkers. Magnetic studies reveal that compounds **1**−**3** show intramolecular antiferromagnetic coupling between Mn(II) and W(V) centers, which produce the typical ferrimagnetic chain behaviors for compounds **1** and **2** but paramagnetic properties for compound **3**. Notably, field-induced metamagnetic behavior was detected for compound **2**, indicating it undergoes a transition from the antiferromagnetic ground state to ferrimagnetic phase above critical dc field.

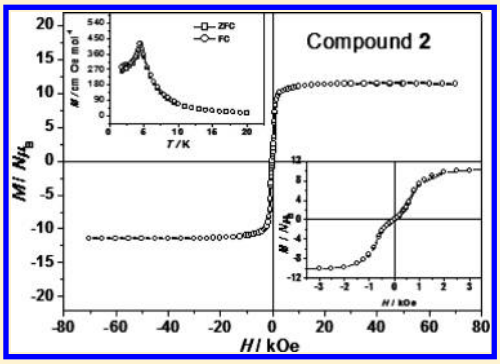

INTRODUCTION

In the past few years, the design and synthesis of coordination compounds have attracted much attention because of their intriguing topologies and fascinating potential applications.[1] Especially, considerable efforts into crystal engineering have been devoted to the design and construction of octacyanometallates $[M(CN)_8]^{3-/4-}$ (M = Mo, W, and Nb)-based magnets.[2,3] Octacyanometallates as versatile building blocks not only can mediate strong coupling interactions between metal centers but also adopt three different spatial configurations depending on the external environment (square antiprism, dodecahedron, and bicapped trigonal prism). The combination of $[M(CN)_8]$ units as carriers of unpaired spin with 3d metal ions has produced various dimensional molecular structures ranging from zero-dimensional (0D) clusters to three-dimensional (3D) networks, and the resulting materials displayed rich magnetic properties such as high T_c values,[4−6] photo-/guest-induced magnetism,[7−10] single molecule or single chain magnets,[11,12] and spin crossover magnetism.[13,14]

From the synthesis point of view, the chelated ligands have been usually used to control the coordination number and spatial arrangement around metal centers for cyanide-bridging, thus resulting in low-dimensional octacyanometallate-based structures rather than extended frameworks, while longer bridging ligands (e.g., polypyridines, pyridyl N-oxides) were used to construct high-dimensional structures.[2] Notably, spacer ligands have been applied in the construction of extended networks from preorganized Mn_9W_6 clusters; for example, $\{Mn_9W_6\}$ clusters could be connected by 4,4′-bipyridine (4,4′-bpy) and *trans*-1,2-di(4-pyridyl)ethene (dpe) linkers into 2D and 3D hybrid networks, respectively.[15,16] Meanwhile, $\{Co_9W_6\}$ clusters were combined with 4,4′-bipyridine-*N*,*N*′-dioxide (4,4′-bpdo) linkers, forming H-bonded supramolecular chains and 1D nanowires.[17] However, how to control rationally the desired structures with specific properties still remains a great challenge. In order to search for effective synthetic strategies of high-dimensional octacyanometallate-based compounds, and then further investigate the structure-magnetism correlations involved in such systems, the in situ and secondary assembly methods were employed recently by our group in the presence of linear bridging ligands dpe and 4,4′-azopyridine (azpy), isolating three manganese(II)-octacyanotungstate(V) bimetallic compounds with 1D or 3D structures: $[Mn(H_2O)_2(dpe)]_3[W(CN)_8]_2\cdot 2dpe\cdot 7H_2O$ (**1**), [Mn-

Received: July 27, 2014
Revised: November 20, 2014

   dx.doi.org/10.1021/cg501128n | *Cryst. Growth Des.* XXXX, XXX, XXX−XXX

Table 1. Crystallographic Data and Structural Refinement for Compounds 1−3

compound	1	2	3
formula	$C_{76}H_{76}Mn_3N_{26}O_{13}W_2$	$C_{76}H_{68}Mn_3N_{40}O_{10}W_2$	$C_{100}H_{86}Mn_3N_{50}O_8W_2$
M_r	2094.15	2234.22	2648.71
crystal system	monoclinic	triclinic	monoclinic
space group	$C2/c$	$P\bar{1}$	$P2_1/c$
a (Å)	12.6227(8)	10.6761(13)	13.6349(12)
b (Å)	24.6013(16)	16.1012(15)	34.8022(13)
c (Å)	32.699(2)	18.0131(15)	12.2471(11)
α (deg)	90.00	103.521(3)	90.00
β (deg)	99.702(2)	106.261(2)	102.085(2)
γ (deg)	90.00	108.668(3)	90.00
V (Å^3)	10009.1(11)	2632.1(5)	5682.8(7)
Z	4	1	2
ρ_{calcd} (g cm^{-3})	1.390	1.410	1.548
μ (mm^{-1})	2.722	2.594	2.418
total, unique	36139, 9648	21134, 9140	54924, 12871
observed [$I > 2\sigma(I)$]	7399	8227	10750
GOF on F^2	1.054	1.072	1.088
R_1, ωR_2 [$I > 2\sigma(I)$]	0.0548, 0.1377	0.0503, 0.1238	0.0565, 0.1458
R_1, ωR_2 (all data)	0.0602, 0.1390	0.0522, 0.1244	0.0588, 0.1468

$(H_2O)_2(azpy)]_3[W(CN)_8]_2\cdot 3azpy\cdot 4H_2O$ (**2**), and $[Mn(H_2O)_3(azpy)]_2[Mn(CH_3CN)_2(azpy)][W(CN)_8]_2\cdot 5azpy\cdot 2H_2O$ (**3**). In this work, the syntheses, crystal structures, and magnetic properties of compounds **1**−**3** were reported.

EXPERIMENTAL SECTION

General Considerations. All chemicals and solvents were purchase from Alfa Aesar and used as received. $Mn(ClO_4)_2\cdot 6H_2O$, *trans*-1,2-di(4-pyridyl)ethene (dpe) ligand were purchased from Alfa Aesar and used without further purification. The $[HN(n\text{-}C_4H_9)_3]_3W(CN)_8$ precursor and 4,4′-azopyridine (azpy) ligand were prepared according to the published procedures.[18,19] Elemental analyses for C, H, and N were performed with a PerkinElmer 240C elemental analyzer. IR spectra were measured on a Nicolet FT 1703X spectrophotometer in the form of KBr pellets from 4000 to 400 cm^{-1}. All magnetic measurements on microcrystalline sample were conducted on a Quantum Design MPMP-XL7 superconducting quantum interference device (SQUID) magnetometer. Corrections of measured susceptibilities were carried out considering both the sample holder as the background and the diamagnetism of the constituent atoms according to Pascal's tables.[20]

Syntheses of $[Mn(H_2O)_2(dpe)]_3[W(CN)_8]_2\cdot 2dpe\cdot 7H_2O$ (1). Single crystals of compound **1** were obtained by the secondary assembly method. A small glass vial (3 mL) containing diethyl ether solvent was placed into a big glass vial (15 mL) containing the solids of $Mn(ClO_4)_2\cdot 6H_2O$ (0.075 mmol, 27.15 mg) and $[HN(n\text{-}C_4H_9)_3]_3W(CN)_8$ (0.05 mmol, 40.55 mg). Then an ethanol solvent (8 mL) was poured slowly into the big vial until the liquid level was just below the small vial. The big vial was sealed, and red-brown crystals (Mn_9W_6 clusters) were obtained after 5 days at room temperature. Second, the solids of above Mn_9W_6 clusters and excess dpe ligands (0.2 mmol, 36.04 mg) were quickly put into small (3 mL) and big (15 mL) glass vials, respectively. Then, an ethanol/water (V/V = 1/1) solution was poured carefully into both vials until the liquid level was over the small vial about 1 cm. Block-shaped red-brown crystals of compound **1** were obtained after one month. IR: $\nu_{C\equiv N}$ = 2172, 2124 cm^{-1}. Anal. Calcd for $C_{76}H_{76}Mn_3N_{26}O_{13}W_2$ (**1**) (%): C, 43.59; H, 3.66; N, 17.39. Found: C, 43.28; H, 3.87; N, 17.83. Yield (based on Mn salt): ∼31%.

Synthesis of $[Mn(H_2O)_2(azpy)]_3[W(CN)_8]_2\cdot 3azpy\cdot 4H_2O$ (2). Substituting azpy for dpe in the synthesis procedure of compound **1** resulted in the formation of rod-shaped red crystals of compound **2**. IR: $\nu_{C\equiv N}$ = 2162, 2116 cm^{-1}. Anal. Calcd for $C_{76}H_{68}Mn_3N_{40}O_{10}W_2$ (**2**) (%): C, 40.86; H, 3.07; N, 25.08. Found: C, 41.11; H, 3.13; N, 24.89. Yield (based on Mn salt): ∼29%.

Syntheses of $[Mn(H_2O)_3(azpy)]_2[Mn(CH_3CN)_2(azpy)][W(CN)_8]_2\cdot 5azpy\cdot 2H_2O$ (3). A small glass vial (3 mL) containing diethyl ether solvent was placed into a big glass vial (15 mL) containing the solids of $Mn(ClO_4)_2\cdot 6H_2O$ (0.075 mmol, 27.15 mg), $[HN(n\text{-}C_4H_9)_3]_3W(CN)_8$ (0.05 mmol, 40.55 mg) and azpy (0.1 mmol, 18.42 mg). Then an acetonitrile/water (V/V = 1/1) solution (8 mL) was poured slowly into the big vial until the liquid level was just below the small vial. The big vial was sealed, and block-shaped red crystals were obtained after 2 weeks at room temperature. The crystals were filtered, washed in acetonitrile/water, and dried in air. IR: $\nu_{C\equiv N}$ = 2162, 2117 cm^{-1}. Anal. Calcd for $C_{100}H_{86}Mn_3N_{50}O_8W_2$ (**3**) (%): C, 45.35; H, 3.27; N, 26.44. Found: C, 45.79; H, 3.16; N, 26.89. Yield (based on Mn salt): ∼36%.

Crystallographic Data Collection and Structural Determination. Diffraction data for compounds **1**−**3** were collected on a Bruker Smart APEX II diffractometer equipped with Mo-K_α (λ = 0.71073 Å) radiation. Diffraction data analysis and reduction were performed within *SMART*, *SAINT*, and *XPREP*.[21] Correction for Lorentz, polarization and absorption effects were performed within *SADABS*.[22] Structures were solved using the Patterson method within *SHELXS-97* and refined using *SHELXL-97*.[23−25] All non-hydrogen atoms were refined with anisotropic thermal parameters. The H atoms of dpe, azpy, and acetonitrile molecules were calculated at idealized positions and included in the refinement in a riding mode. The H atoms bound to water molecules were located from difference Fourier maps and refined as riding. The O6W−O11W atoms of water molecules in the structure of compound **1** are all disordered and have the same occupancy of 0.25, while the O4W−O8W atoms of water molecules in compound **2** have different occupancies of 0.30−0.50. The crystallographic data and structural refinement for compounds **1**−**3** are summarized in Table 1. Selected bond distances and angles are listed in Table 2. The full structures of compounds **1**−**3** are provided in the Supporting Information (Figures S4−S6). Crystallographic data of compounds **1**, **2**, and **3** have been deposited at the Cambridge Crystallographic Data Centre as CCDC numbers 991486, 991487, and 991488, respectively.

RESULTS AND DISCUSSION

Syntheses. To organize M_9W_6 (M = Mn, Co) clusters into coordination assemblies, spacer ligands such as 4,4′-bpy, dpe, or 4,4′-bpdo have been employed successfully in the assembling of hybrid networks.[15−17] Following this approach, we also applied this assembly method in the syntheses of our products. However, the target compounds were not obtained. When the

dx.doi.org/10.1021/cg501128n | Cryst. Growth Des. XXXX, XXX, XXX−XXX

Table 2. Selected Bond Distances (Å) and Angles (°) for Compounds 1−3[a]

1		2		3	
C1−W1	2.189(6)	C1−W1	2.129(5)	C1−W1	2.140(5)
C2−W1	2.174(7)	C2−W1	2.185(5)	C2−W1	2.147(5)
C3−W1	2.155(7)	C3−W1	2.113(5)	C3−W1	2.178(5)
C4−W1	2.184(7)	C4−W1	2.145(6)	C4−W1	2.140(5)
C5−W1	2.157(6)	C5−W1	2.132(5)	C5−W1	2.143(4)
C6−W1	2.152(7)	C6−W1	2.182(5)	C6−W1	2.147(5)
C7−W1	2.162(7)	C7−W1	2.177(5)	C7−W1	2.170(4)
C8−W1	2.184(7)	C8−W1	2.192(6)	C8−W1	2.175(5)
C1−N1	1.132(8)	C1−N1	1.189(7)	C1−N1	1.156(7)
C2−N2	1.149(8)	C2−N2	1.157(6)	C2−N2	1.157(6)
C3−N3	1.146(8)	C3−N3	1.177(6)	C3−N3	1.148(7)
C4−N4	1.128(8)	C4−N4	1.160(7)	C4−N4	1.157(6)
C5−N5	1.173(8)	C5−N5	1.161(6)	C5−N5	1.185(6)
C6−N6	1.182(8)	C6−N6	1.171(6)	C6−N6	1.159(7)
C7−N7	1.157(8)	C7−N7	1.161(7)	C7−N7	1.150(6)
C8−N8	1.135(8)	C8−N8	1.150(8)	C8−N8	1.141(6)
N4−Mn1	2.209(6)	N1−Mn1	2.215(4)	N1−Mn1	2.219(4)
N11−Mn1	2.241(5)	$N5^{i}$−Mn1	2.227(4)	N10−Mn1	2.339(4)
O1W−Mn1	2.211(4)	N9−Mn1	2.228(4)	$N13^{i}$−Mn1	2.331(4)
N1−Mn2	2.225(6)	N13−Mn1	2.133(4)	O1W−Mn1	2.174(4)
N9−Mn2	2.246(5)	O1W−Mn1	2.224(3)	O2W−Mn1	2.144(3)
$N10^{iii}$−Mn2	2.230(5)	O2W−Mn1	2.155(3)	O3W−Mn1	2.151(3)
$N3^{iv}$−Mn2	2.237(6)	$N2^{iv}$−Mn2	2.198(4)	N2−Mn2	2.201(4)
O2W−Mn2	2.163(4)	N12−Mn2	2.240(4)	N9−Mn2	2.256(4)
O3W−Mn2	2.226(4)	O3W−Mn2	2.167(4)	N14−Mn2	2.307(4)
N1−C1−W1	179.0(6)	N1−C1−W1	175.8(4)	N1−C1−W1	179.2(5)
N2−C2−W1	178.0(6)	N2−C2−W1	176.3(4)	N2−C2−W1	177.0(4)
N3−C3−W1	174.0(6)	N3−C3−W1	176.6(5)	N3−C3−W1	179.2(5)
N4−C4−W1	179.2(6)	N4−C4−W1	174.0(5)	N4−C4−W1	179.1(5)
N5−C5−W1	176.6(6)	N5−C5−W1	176.2(4)	N5−C5−W1	179.3(5)
N6−C6−W1	179.0(6)	N6−C6−W1	177.2(5)	N6−C6−W1	178.0(5)
N7−C7−W1	179.0(7)	N7−C7−W1	175.3(4)	N7−C7−W1	178.4 (4)
N8−C8−W1	172.9(6)	N8−C8−W1	178.9(5)	N8−C8−W1	179.2(4)
C4−N4−Mn1	176.4(5)	C1−N1−Mn1	176.4(4)	C1−N1−Mn1	154.2(4)
C1−N1−Mn2	170.9(5)	$C5−N5−Mn1^{vi}$	156.6(4)	C2−N2−Mn2	157.2(4)
$C3−N3−Mn2^{iv}$	168.2(5)	$C2−N2−Mn2^{v}$	169.8(4)		

[a]Symmetry codes for compound **1**: (iii) $x + 1/2, y + 1/2, z$. (iv) $-x, y, -z + 1/2$; for compound **2**: (i) $x + 1, y, z$; (iv) $x, y - 1, z$; (v) $x, y + 1, z$; (vi) $x - 1, y, z$; for compound **3**: (i) $x + 1, y, z$.

preorganized Mn_9W_6 clusters were used to react with spacer ligands (dpe, azpy), unexpectedly 3D Mn(II)−W(V) compounds **1** and **2** were isolated instead of Mn_9W_6-based hybrid networks. No clusters were found in the structures of both compounds, and the reason was not clear. Notably, the 3D networks were formed through the cross-link of 1D infinite 3,2-chains and rope-ladder chains with linear ligands for compounds **1** and **2**, respectively. When the assembly method and reaction solvents changed, compound **3** with 1D structure was obtained. These results showed spacer ligands, the assembly process, and solvents played an important role in the formation of compounds **1**−**3**.

Crystal Structures. Single crystal X-ray diffraction results show that compound **1** crystallizes in the monoclinic space group $C2/c$ and shows a 3D network through the cross-link of 1D infinite 3,2-chains with linear ligand dpe. The asymmetric unit consists of three $[Mn(H_2O)_2(dpe)]^{2+}$ cations, two $[W(CN)_8]^{3-}$ anions, two noncoordinated dpe ligands, and seven crystallized water molecules (Figure 1). The W atom adopted a slightly distorted square antiprism geometry, in which three cyanide groups bridged to the neighboring Mn centers and the others are terminal. The W1−C and C−N bond distances range from 2.151(7) to 2.189(6) Å and from 1.128(8) to 1.182(8) Å, respectively, while all W1−CN units are almost linear with the maximum deviation from linearity of 7.1°. The coordination parameters of the W center are typical of octacyanotungstates.[26−29] The $[Mn(H_2O)_2(dpe)]$ moiety is comprised two independent Mn centers (Mn1 and Mn2). The Mn1 atom is six-coordinated by two *trans* dpe ligands, two *trans* bridged CN groups, and two water molecules in the *trans* arrangement, with an octahedral $\{Mn1N_4O_2\}$ geometry. The Mn1−N4 and Mn1−N11 bond distances are 2.209(6) and 2.241(5) Å, respectively, and the Mn1−O1W bond length is 2.211(4) Å. The coordinated geometry around the Mn2 center is different from that around Mn1. Two water molecules coordinated to Mn2 atom in the octahedral $\{Mn2N_4O_2\}$ unit exhibits the cis arrangement. Furthermore, the dihedral angle of two aromatic rings from dpe ligand coordinated to Mn2 atom is about 24.25°, while two rings observed in Mn1 center are in the same plane.

As shown in Figure 2, the W1 and Mn2 centers are connected alternatively by cyanide bridges to generate a four-

dx.doi.org/10.1021/cg501128n | *Cryst. Growth Des.* XXXX, XXX, XXX−XXX

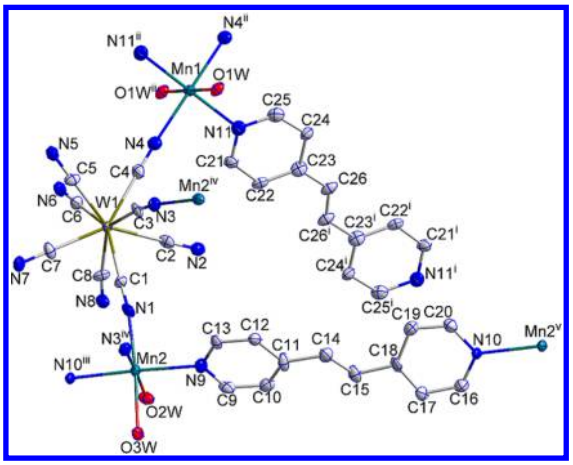

Figure 1. *ORTEP* diagram of compound **1** with displacement ellipsoids of 30% probability level. Hydrogen atoms, crystallized water molecules and noncoordinated dpe ligands were omitted for clarity. Symmetry codes: (i) $-x + 1/2, -y + 3/2, -z + 1$; (ii) $-x, -y + 2, -z + 1$; (iii) $x + 1/2, y + 1/2, z$. (iv) $-x, y, -z + 1/2$; (v) $x - 1/2, y - 1/2, z$.

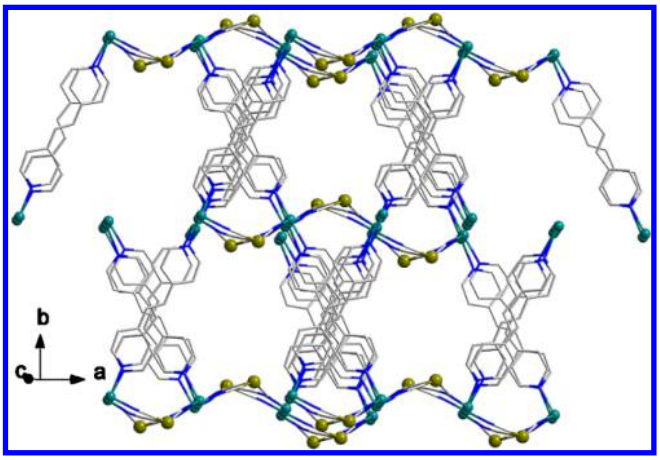

Figure 3. 3D network for compounds **1**. All hydrogen atoms, water molecules, terminal cyanide groups, and noncoordinated dpe ligands were omitted for clarity.

metallic 12-atom rhombic ring, $Mn_2W_2(CN)_4$ (Figure 2), where W1 and Mn2 atoms are located on the vertexes, while cyanide groups form the sides. The diagonal dimensions of the rhombus are approximately 8.335 Å (W1···W1) and 6.403 Å (Mn2···Mn2). Then Mn1 atoms as linkers bridge adjacent rings in the *trans* mode through -NC−Mn1−CN- linkages, forming an infinite 3,2-chain along the *c* axis. The Mn1···Mn1 distances between the adjacent Mn_3W_2 chains along the *a* and *b* axis are 12.623 and 13.825 Å, respectively, while the Mn1···Mn1 distance in the chain is about 16.350 Å. The 3,2-chain structure of compound **1** has also been documented in related cyanide-based compounds.[30−32]

As a result, the chains are further cross-linked by dpe ligands running along two different directions (33.911° of torsion angle), generating a 3D network (Figure 3), in which noncoordinated dpe ligands and crystallized water molecules are trapped. It should be noted here that the 3,2-chains in compound $[Cu(\mu\text{-}4,4'\text{-bpy})(DMF)_2][Cu(\mu\text{-}4,4'\text{-bpy})(DMF)]_2[W(CN)_8]_2\cdot 2DMF\cdot 2H_2O$ are linked by 4,4′-bpy along the same [0 0 1] direction, forming a 2D grid layer.[33] The structural difference between both compounds may be reasonably attributed to distinct connection directions of linear ligands. Terminal cyanide ligands, coordinated and uncoordinated water molecules, and crystallized dpe ligands are all involved in the formation of the hydrogen-bonding network. Uncoordinated water molecules interact with terminal cyanide ligands through O−H···N hydrogen bonds, while the coordinated water molecules interact with uncoordinated water by O−H···O hydrogen bonds. Simultaneously, the coordinated water molecules interact with uncoordinated dpe ligands through the O−H···N hydrogen bonds.

The structures of compounds **1** and **2** are significantly distinct, although crystals of both products are synthesized under similar conditions except for linear ligands. Different from the monoclinic *C*2/*c* for compound **1**, compound **2** crystallizes in the triclinic space group $P\bar{1}$ and shows a 3D framework through the cross-link of rope-ladder chains with linear ligand azpy. The asymmetrical unit contains three $[Mn(H_2O)_2(azpy)]^{3+}$ cations, two $[W(CN)_8]^{3-}$ anions, three noncoordinate azpy ligands, and four crystallized water molecules (Figure 4). The W1 center adopts a distorted square antiprism consisting of eight CN groups with the W1−C bond length ranging from 2.113(5) to 2.192(6) Å and a maximum deviation of the W1-CN angle from linearity of 6.0°. Three cyanide groups bridged to neighboring Mn centers and the others are terminal. Both Mn1 and Mn2 centers are situated in a distorted slightly octahedral $\{MnN_4O_2\}$ geometry. As shown in Figure 5, the W and Mn atoms are linked alternatively through cyanide bridges to form a rope-ladder chain, different from the 3,2-chain for compound **1**. A careful comparison of compounds **1** and **2** shows that the type of linear ligands has an obvious influence on the final structures. In fact, this type of 1D rope-ladder chain is reminiscent of hexa- and octacyanometate-based systems.[34,35]

Then, neighboring rope-ladder chains are further cross-linked by azpy ligands (the -Mn2-azpy-Mn1- and -Mn1-azpy-Mn1-linkages), resulting in the formation of a 3D network (Figure 6). The Mn1···Mn1, Mn1···Mn2, and W1···W1 distances between adjacent chains are about 13.4733, 13.468, and 13.229 Å, respectively. Terminal cyanide ligands, coordinated water molecules, and crystallized azpy ligands in compound **2** are involved in the formation of the hydrogen-bonding network. Coordinated water molecules interact with terminal cyanide ligands or uncoordinated azpy ligands through O−H···N hydrogen bonds.

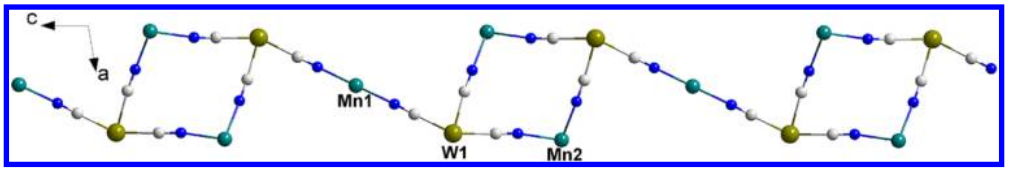

Figure 2. 1D 3,2-chain structure for compound **1** along the *c* axis. All hydrogen atoms, water molecules, terminal cyanide groups, and dpe ligands were omitted for clarity.

dx.doi.org/10.1021/cg501128n | *Cryst. Growth Des.* XXXX, XXX, XXX−XXX

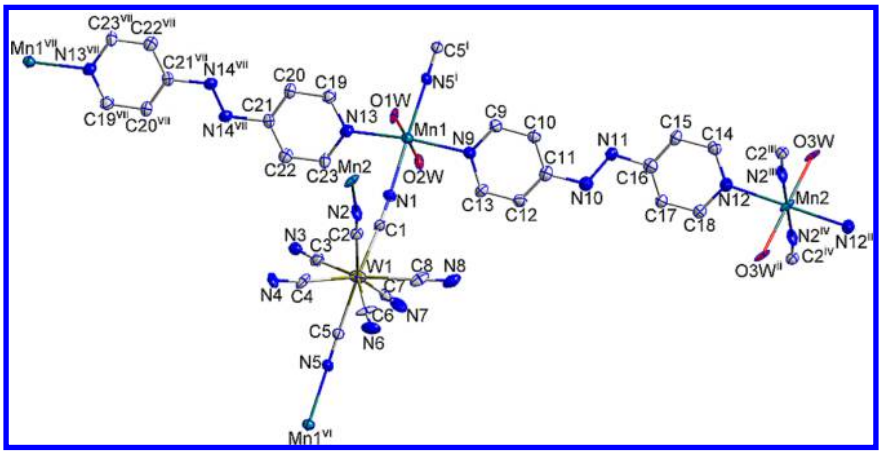

Figure 4. *ORTEP* diagram of compound **2** with displacement ellipsoids of 30% probability level. Hydrogen atoms, crystallized water molecules, and noncoordinated azpy ligands were omitted for clarity. Symmetry codes: (i) $x + 1, y, z$; (ii) $-x + 1, -y - 1, -z + 1$; (iii) $-x + 1, -y, -z + 1$; (iv) $x, y - 1, z$; (vi) $x - 1, y, z$; (vii) $-x + 1, -y + 1, -z$.

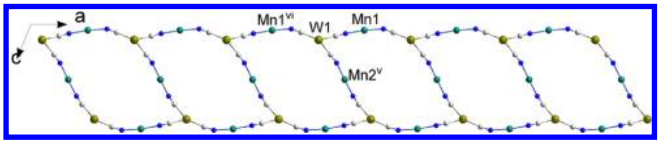

Figure 5. 1D rope-ladder chain structure of compound **2**. All hydrogen atoms, azpy ligands, and crystallized water molecules were omitted for clarity. Symmetry codes: (v) $x, y + 1, z$; (vi) $x - 1, y, z$.

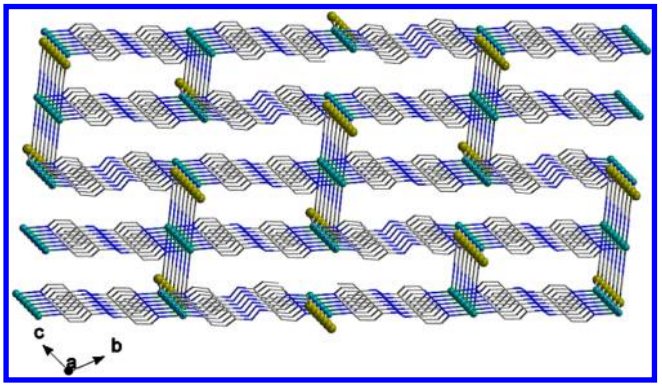

Figure 6. 3D network for compound **2** viewed from the *a* axis. All hydrogen atoms, water molecules, noncoordinated azpy ligands, and terminal cyanide groups were omitted.

Compound **3** crystallizes in the monoclinic space group $P2_1/c$ and adopts a 1D ribbon structure by the connection of pentanuclear repeating units with azpy linkers. To the best of our knowledge, the ribbon-like structure observed in our case has not been documented in octacyanometallate-based system so far. The asymmetrical unit contains two $[Mn(H_2O)_3(azpy)]^{2+}$ cations, one $[Mn(CH_3CN)_2(azpy)]^{2+}$ cation, two $[W(CN)_8]^{3-}$ anions, five noncoordinated azpy ligands, and two crystallized water molecules (Figure 7).

The geometry of the W atom surrounded by eight CN ligands is determined as a distorted square antiprism. Two *trans* cyanide groups bridged to two adjacent Mn centers, and the others are terminal. Both the crystallographically independent Mn1 and Mn2 atoms take a distorted slightly octahedral configuration. The coordinated sites of Mn1 atom are filled by one cyanide group, two *trans* azpy ligands, and three water molecules, while Mn2 atom is occupied by two cyanide groups, two *trans* azpy ligands, and two CH_3CN molecules. As shown

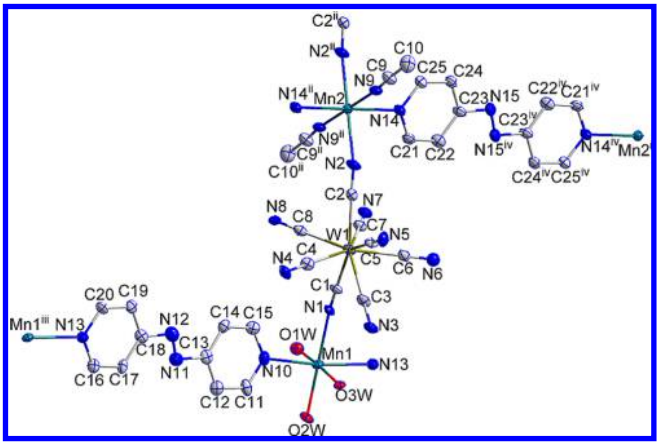

Figure 7. *ORTEP* diagram of compound **3** with displacement ellipsoids of 30% probability level. Hydrogen atoms, crystallized water molecules, and noncoordinated dpe ligands have been omitted for clarity. Symmetry codes: (i) $x + 1, y, z$; (ii) $-x + 1, -y + 1, -z + 1$; (iii) $x - 1, y, z$; (iv) $-x + 2, -y + 1, -z + 1$.

in Figure 8, the Mn and W atoms are linked alternatively through cyanide bridges to form a pentanuclear repeating unit

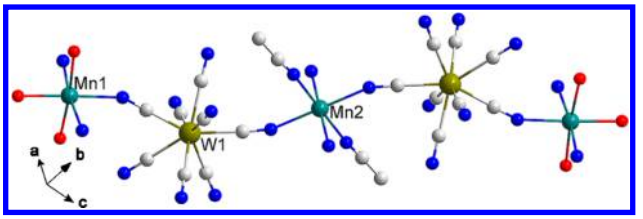

Figure 8. Pentanuclear repeating unit of compound **3**. All hydrogen atoms, water molecules, and azpy ligands were omitted for clarity.

with the length of 20.598 Å (Mn1···Mn1 distance). Thus, the adjacent chains are further connected along the *a* axis by *trans* azpy ligands to generate a ribbon-like structure (Figure 9). The lattice water molecules and noncoordinated azpy ligands are filled between the ribbons. In the network of compound **3**, coordinated water molecules interact with terminal cyanide ligands or uncoordinated azpy ligands through O−H···N hydrogen bonds. Furthermore, the uncoordinated water molecules also interact with terminal cyanide groups through

dx.doi.org/10.1021/cg501128n | *Cryst. Growth Des.* XXXX, XXX, XXX−XXX

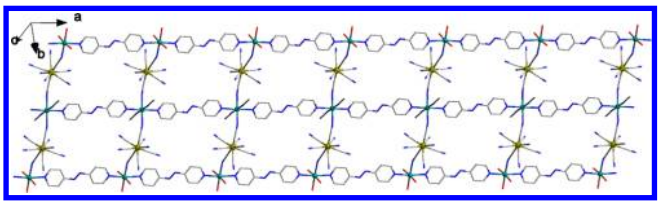

Figure 9. 1D ribbon-like structure of compound **3**. All H atoms, crystallized H_2O molecules, and noncoordinated azpy ligands were omitted for clarity.

the O−H···N hydrogen bonds. The distance of neighboring ribbons is equal to 13.635 Å (Mn1···Mn1 distance).

Magnetic Properties. The measurements of variable-temperature magnetic susceptibilities were performed on polycrystalline samples of compounds **1**−**3** from 1.8 to 300 K in a typical applied field of 2 kOe. Because of the metamagnetic-like properties of compound **2**, further measurement of the susceptibility data of compound **2** was carried out (1.8−15 K) in various applied dc fields ranging from 2 kOe to 0.2 kOe. For compound **2**, the susceptibility measured at high field (higher than 1k Oe) might prevent the metamagnetic magnetic phase transition at very low temperature, but this influence could be safely neglected in a high temperature region. So, all the data of compounds **1**−**3** collected in 2 kOe were plotted for general discussion. As shown in Figure 10a,c,e, the $\chi_M T$ values (per $Mn^{II}_3W^{V}_2$) of compounds **1**−**3** at room temperature are 12.63, 14.49, and 12.88 cm^3 K mol^{-1}, respectively, which are overall consistent with the spin-only value of 13.87 cm^3 K mol^{-1} calculated for the $Mn^{II}_3W^{V}_2$ unit

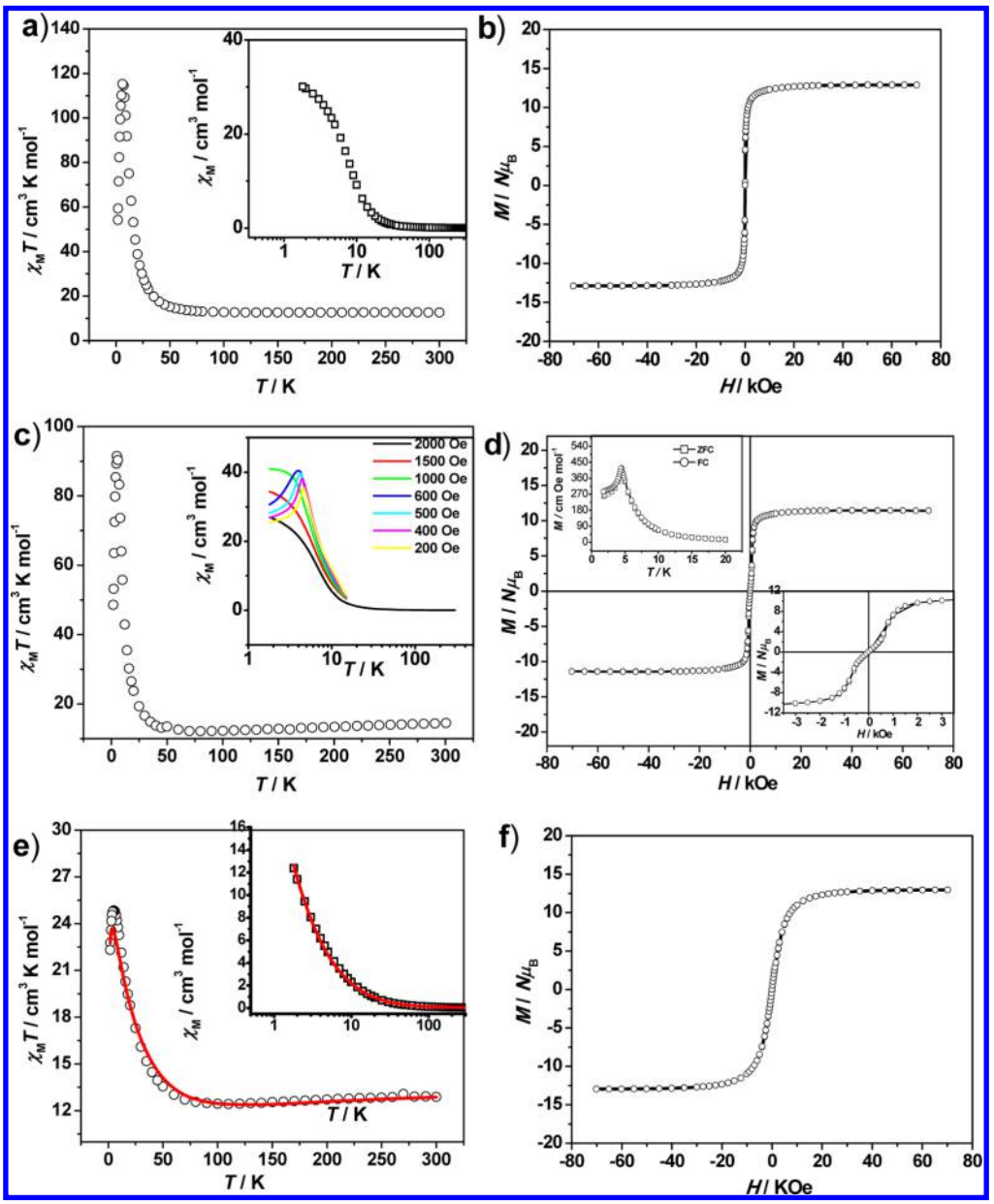

Figure 10. Temperature dependence of $\chi_M T$ for compounds **1** (a), **2** (c), and **3** (e) measured at 2 kOe (the insets are χ_M vs T curves for compounds **1**−**3**; the red solid line in $\chi_M T$ vs T curve of compound **3** represents the best fit of the magnetic data using the model described in the text); field dependence of the magnetization for compounds **1** (b), **2** (d), and **3** (f) at 1.8 K. (The insets include FC, ZFC magnetization and the hysteresis loop for compound **2**.)

dx.doi.org/10.1021/cg501128n | *Cryst. Growth Des.* XXXX, XXX, XXX−XXX

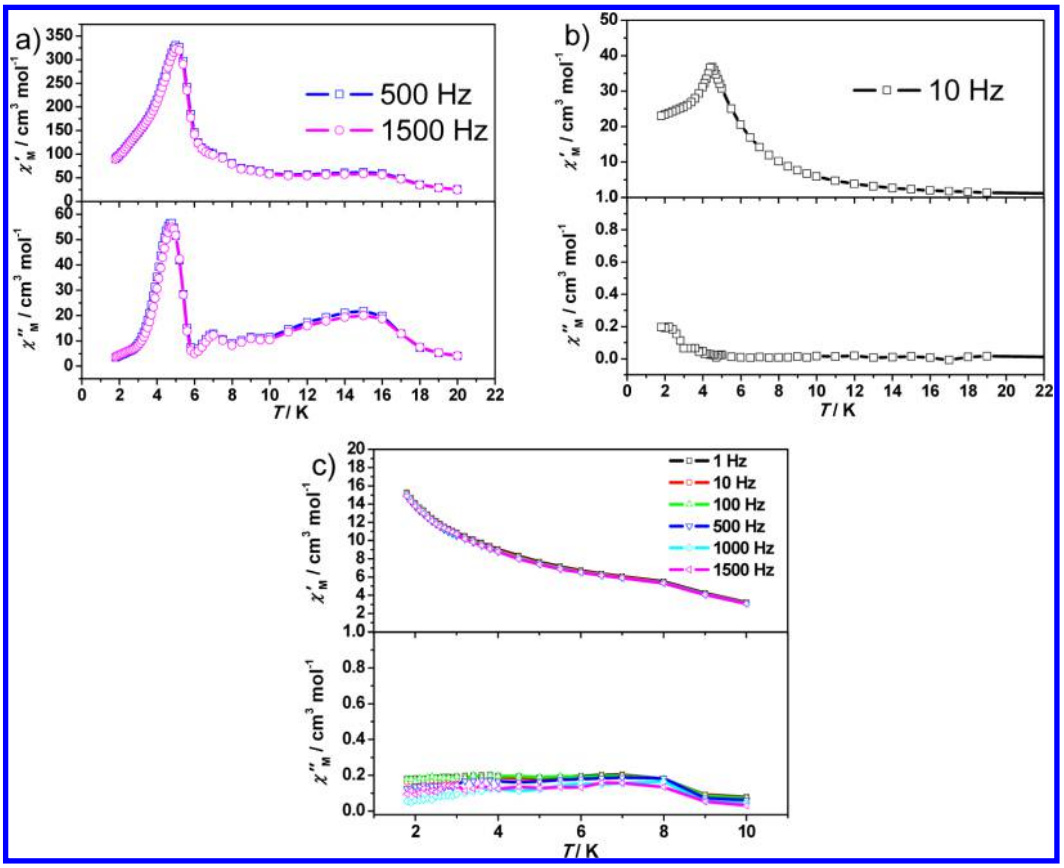

Figure 11. Variable-temperature ac magnetic susceptibility for compounds **1** (a) (H_{dc} = 0, f = 500, 1500 Hz, and H_{ac} = 3 Oe), **2** (b) (H_{dc} = 0, f = 10 Hz, and H_{ac} = 3 Oe), and **3** (c) (H_{dc} = 0, f = 1, 10, 100, 500, 1000, 1500 Hz, and H_{ac} = 3 Oe).

(S_W = 1/2, S_{Mn} = 5/2) assuming g_W = g_{Mn} = 2.0. As revealed by previous studied W^V−CN−Mn^{II} systems,[36−44] antiferromagnetic interactions between W^V and Mn^{II} ions are always observed, and thus the room temperature $\chi_M T$ values are often slightly smaller than spin-only ones.

Upon cooling, the $\chi_M T$ value of compound **1** keeps almost constant, while that for compound **2** decreases gradually. But as the system further cools down, an abruptly increase of the $\chi_M T$ values was observed with the values changing from 12.77 to 115.26 cm^3 K mol^{-1} for compound **1** and 12.25 to 91.48 cm^3 K mol^{-1} for compound **2**, respectively. Such behaviors are obviously an indication of the long-range magnetic ordering resulting from the interaction between W^V and Mn^{II} ions. Finally, the $\chi_M T$ values of compounds **1** and **2** again decrease until they reach 54.20 and 48.54 cm^3 K mol^{-1} at 1.8 K. No maximum was detected in the χ_M vs T curve measured at 2 kOe (inset of Figure 10a,c), the downturn of the values at very low temperature could be ascribed to the saturation effect and/or intermolecular antiferromagnetic interactions. The $\chi_M T$ vs T curve of compound **3** shows mainly a comparable feature to compounds **1** and **2**, but no abruptly increase of the $\chi_M T$ values was observed at the low temperature region. The Curie−Weiss fitting for compounds **1**−**3** between 100 and 300 K gives the Weiss constants of 1.2(4) K, −27.1(22) K, and −6.2(5) K, respectively. It is still insufficient to claim that the intramolecular W^V···Mn^{II} interactions are antiferromagnetic (AF). However, associated with the ferrimagnetic properties of other cyanide bridged W^V···Mn^{II} compounds with extended structures,[45,46] the negative Weiss constants might be an indication of the antiferromagnetic W^V···Mn^{II} interactions presented in compounds **2** and **3**. The very small positive Weiss constant of compound **1** observed should be taken with caution because it is contradictory to the well-known AF nature of W^V···Mn^V interactions. Such unconventional phenomena were also observed in the literature,[15,16,45,47] and one reasonable explanation is that the large diffusion of the 4d and 5d orbital leads to coupling interaction in a wide range of temperature, and thus the minimum of the $\chi_M T$ curve for antiferromagnetic coupled W^V and Mn^{II} ions might become very broad or even at higher temperatures than room temperature.

To the best of our knowledge, no available suitable theoretical models could be used for evaluating quantitatively the magnitude and sign of the magnetic coupling constants in such complicated systems of compounds **1**−**3**. However, the magnetostructural correlations could be qualitatively described. From the structural analysis result, compounds **1** and **2** show such peculiar 3D topological structures. Actually, the structures could be simplified as 1D Mn−W chains that are tied together by the organic ligands. From the magnetic point of view, the magnetic exchanges mediated by the CN bridges would be much stronger than that for organic ligands pathways because the latter produce very long separations between the spin carriers. On the basis of the above assumptions, the $\chi_M T$ vs T behaviors of compounds **1** and **2** are actually governed by the ferrimagnetic Mn−W chains, while compound **3** is simply 0D spin clusters. Therefore, the decreases of the $\chi_M T$ at the high temperature region are a unanimously short-range order state where the spins of adjacent Mn and W are antiparallel arranged. As the temperature further decreases, the correlation length

dx.doi.org/10.1021/cg501128n | *Cryst. Growth Des.* XXXX, XXX, XXX−XXX

within the chains increases, and the onset of ordering of the uncompensated spins further leads to the abrupt increase of the $\chi_M T$ values. For compound **3**, the 1D ribbon structures are actually composed of 1D weakly connected pentanuclear repeating units of Mn_3W_2. From this point of view, the lack of an abrupt increase of $\chi_M T$ values for compound **3** is logical and could be further confirmed by the rough simulation of the susceptibility data by simplifying compound **3** as a linear pentanuclear Mn_3W_2 unit. On the basis of the Hamiltonian $\hat{H} = -2JS_{Mn1}S_{W1} - 2JS_{Mn2}S_{W1} - 2JS_{Mn2}S_{W2} - 2JS_{Mn3}S_{W2}$ (J represents the intramolecular coupling constant of Mn···W interactions), the $\chi_M T$ vs T plot of compound **3** could be well reproduced down to 1.8 K by running the Magpack program,[48] affording the best match of parameters: $J = -15$ cm^{-1}, $g = 2.0$. The simulation result further indicates that the magnetic behavior of compound **3** is actually determined by the antiferromagnetic coupled pentanuclear Mn_3W_2 unit.

Variable-field magnetization (−70−70 kOe) was then measured for compounds **1**−**3** to verify their behaviors. As shown in Figure 10b,d,f, compounds **1** and **2** are very easily magnetized, and the magnetizations rapidly increase and reach the saturation value of 12.88 and 11.40 $N\mu_B$ at 70 kOe. The saturation values correspond to the theoretical value (13 $N\mu_B$, calculated from $M_S = g(3S_{Mn} - 2S_W)$ with $g = 2.0$) for the antiferromagnetic coupled Mn_3W_2 unit, further confirming the AF nature. Different from compounds **1** and **2**, the $M-H$ curve of compound **3** increases moderately until reaching the saturation magnetization value of 12.95 $N\mu_B$ at 70 kOe, which also supports the AF nature of intramolecular magnetic coupling. None of the three compounds show obvious hysteresis loops even at 1.8 K (Figure 10b,d,f), precluding their ferrimagnet properties. It is well-known that the hysteresis loops are related to the structural dimensions in which high dimensions often lead to higher Curie temperature and larger hysteresis loops. Consequently, the lack of a hysteresis effect in $M-H$ measurements for such ferrimagnetic systems further prove that these compounds are indeed structurally 3D networks but should be better treated as 1D or 0D systems at least from the magnetic point of view.

Interestingly, the magnetization curve of compound **2** shows a typical sigmoid shape (Figure 10d), and the critical field (H_c) in 1.8 K was determined to be at about 0.6 kOe (location from the maximum of dM/dH vs H plot as shown in Figure S7). The field induced metamagnetic property could further be confirmed by the measurement of field-cooling magnetization (FCM) under differently applied fields in the range of 1.8−15 K. As shown in the inset of Figure 10c, the susceptibility curves show peaks at about 4−5 K, corresponding to the antiferromagnetic phase transition temperature (T_N). Above 0.6 kOe the peaks become less prominent and invisible, confirming the presence of metamagnetic transitions induced by the external fields. Associating with the butterfly M vs H curves and the FC and ZFC measurements (inset of Figure 10d), compound **2** could be considered as typical metamagnetic materials induced by the field from the antiferromagnet gound state to the ferrimagnetic property. To confirm the possible magnetic phase transition at very low temperature, ac magnetic susceptibility was measured (Figure 11). For compound **1**, a frequency independent maximum in the real part was observed at about 5 K accompanied by the corresponding signal in the imaginary part. The result confirms the ferrimagnetic ordering of compounds **1** with the critical temperature (T_c) at about 5 K. For compound **2**, a maximum in χ_M' was also detected at about 4.5 K but no obvious signal in the χ_M'' vs T curve was observed, suggesting that the occurrence of antiferromagnetic ordering below this temperature, which might be caused by the interunit antiferromagnetic interactions.[49] As expected, no detectable ac signal can be observed for compound **3** in the whole temperature explored, which is consistent with the dc magnetic data, revealing the absence of any magnetic transition in compound **3**.

CONCLUSIONS

In summary, three manganese(II)-octacyanotungstate(V) bimetallic compounds **1**−**3** were isolated by in situ or secondary assembly methods. Structural and magnetic analyses reveal that compounds **1** and **2** show a 3D network with dominant antiferromagnetic couplings between Mn(II) and W(V), which promote the formation of novel peculiar ferrimagnetic $(Mn_3W_2)_n$ chains. Interestingly, the field induced metamagnetic property was observed for compound **2**, and compound **3** shows an interesting 1D ribbon structure which could be considered as the 1D arrangement of Mn_3W_2 spin clusters. Although Mn_9W_6 cluster-based compounds were not isolated in the present work, the research along this line is underway, and more useful synthetic strategies will be carried out soon in our lab.

ASSOCIATED CONTENT

Supporting Information

IR spectra and X-ray crystallographic data in CIF format of compounds **1**−**3**. CCDC reference numbers: 991486 (**1**), 991487 (**2**) and 991488 (**3**). This material is available free of charge via the Internet at http://pubs.acs.org.

AUTHOR INFORMATION

Corresponding Authors

*(A.-H.Y.) Tel: +86 511 85639001. Fax: +86 511 85635850. E-mail: aihua.yuan@just.edu.cn.

*(Y.S.) E-mail: yousong@nju.edu.cn.

Notes

The authors declare no competing financial interest.

ACKNOWLEDGMENTS

The authors are grateful for financial support from the National Natural Science Foundation of China (51072072, 51102119, and 51272095), Natural Science Foundation of Jiangsu Province of China (BK2011518), and Qing Lan Project of Jiangsu Province.

REFERENCES

(1) Zhou, H. C.; Long, J. R.; Yaghi, O. M. *Chem. Rev.* **2012**, *112*, 673−674.

(2) Nowicka, B.; Korzeniak, T.; Stefańczyk, O.; Pinkowicz, D.; Chorąży, S.; Podgajny, R.; Sieklucka, B. *Coord. Chem. Rev.* **2012**, *256*, 1946−1971.

(3) Sieklucka, B.; Podgajny, R.; Korzeniak, T.; Nowicka, B.; Pinkowicz, D.; Kozieł, M. *Eur. J. Inorg. Chem.* **2011**, 305−326.

(4) Wang, T. W.; Wang, J.; Ohkoshi, S.; Song, Y.; You, X. Z. *Inorg. Chem.* **2010**, *49*, 7756−7763.

(5) Kosaka, W.; Imoto, K.; Tsunobuchi, Y.; Ohkoshi, S. *Inorg. Chem.* **2009**, *48*, 4604−4606.

(6) Pinkowicz, D.; Podgajny, R.; Bałanda, M.; Makarewicz, M.; Gaweł, B.; Łasocha, W.; Sieklucka, B. *Inorg. Chem.* **2008**, *47*, 9745−9747.

(7) Ohkoshi, S.; Ikeda, S.; Hozumi, T.; Kashiwagi, T.; Hashimoto, K. *J. Am. Chem. Soc.* **2006**, *128*, 5320−5321.
(8) Mathonière, C.; Podgajny, R.; Guionneau, P.; Labrugere, C.; Sieklucka, B. *Chem. Mater.* **2005**, *17*, 442−449.
(9) Herrera, J. M.; Marvaud, V.; Verdaguer, M.; Marrot, J.; Kalisz, M.; Mathonière, C. *Angew. Chem., Int. Ed.* **2004**, *43*, 5468−5471.
(10) Pinkowicz, D.; Podgajny, R.; Gaweł, B.; Nitek, W.; Łasocha, W.; Oszajca, M.; Czapla, M.; Makarewicz, M.; Bałanda, M.; Sieklucka, B. *Angew. Chem., Int. Ed.* **2011**, *50*, 3973−3977.
(11) Lim, J. H.; Yoon, J. H.; Kim, H. C.; Hong, C. S. *Angew. Chem., Int. Ed.* **2006**, *45*, 7424−7426.
(12) Venkatakrishnan, T. S.; Sahoo, S.; Bréfuel, N.; Duhayon, C.; Paulsen, C.; Barra, A.; Ramasesha, S.; Sutter, J. P. *J. Am. Chem. Soc.* **2010**, *132*, 6047−6056.
(13) Ohkoshi, S.; Imoto, K.; Tsunobuchi, Y.; Takano, S.; Tokoro, H. *Nat. Chem.* **2011**, *3*, 564−569.
(14) Arai, M.; Kosaka, W.; Matsuda, T.; Ohkoshi, S. *Angew. Chem., Int. Ed.* **2008**, *47*, 6885−6887.
(15) Podgajny, R.; Nitek, W.; Rams, M.; Sieklucka, B. *Cryst. Growth Des.* **2008**, *8*, 3817−3821.
(16) Podgajny, R.; Choray, S.; Nitek, W.; Rams, M.; Balanda, M.; Sieklucka, B. *Cryst. Growth Des.* **2010**, *10*, 4693−4696.
(17) Chorazy, S.; Podgajn, R.; Nitek, W.; Rams, M.; Ohkoshi, S.; Sieklucka, B. *Cryst. Growth Des.* **2013**, *13*, 3036−3045.
(18) Bok, L. D. C.; Leipoldt, J. G.; Basson, S. S. *Z. Anorg. Allg. Chem.* **1975**, *415*, 81−83.
(19) Brown, E. V.; Granneman, G. R. *J. Am. Chem. Soc.* **1975**, *97*, 621−627.
(20) Kahn, O. *Molecular Magnetism*; VCH Publishers: New York, 1993.
(21) *SMART, SAINT, and XPREP: Area Detector Control and Data Integration and Reduction Software*; Bruker Analytical X-ray Instruments Inc.: Madison, Wisconsin, USA, 1995.
(22) Sheldrick, G. M. *SADABS: Empirical Absorption and Correction Software*; University of Göttingen: Göttingen, Germany, 1996.
(23) Sheldrick, G. M. *SHELXS-97. Program for X-ray Crystal Structure Determination*; Göttingen University: Göttingen, Germany, 1997.
(24) Sheldrick, G. M. *SHELXL-97. Program for X-ray Crystal Structure Determination*; Göttingen University: Göttingen, Germany, 1997.
(25) Sheldrick, G. M. *Acta Crystallogr.* **2008**, *A64*, 112−122.
(26) Wang, J.; Xu, Y. L.; Zhou, H. B.; Wang, H. S.; Song, X. J.; Song, Y.; You, X. Z. *Dalton Trans.* **2010**, *39*, 3489−3494.
(27) Yuan, A. H.; Qian, S. Y.; Liu, W. Y.; Zhou, H.; Song, Y. *Dalton Trans.* **2011**, *40*, 5302−5306.
(28) Zhou, H.; Yuan, A. H.; Qian, S. Y.; Song, Y.; Diao, G. W. *Inorg. Chem.* **2010**, *49*, 5971−5976.
(29) Yoon, J. H.; Lim, J. H.; Choi, S. W.; Kim, H. C.; Hong, C. S. *Inorg. Chem.* **2007**, *46*, 1529−1531.
(30) Withers, J. R.; Li, D. F.; Triplet, J.; Ruschman, C.; Parkin, S.; Wang, G. B.; Yee, G. T.; Holmes, S. M. *Polyhedron* **2007**, *26*, 2353−2366.
(31) Li, D. F.; Zheng, L. M.; Zhang, Y. Z.; Huang, J.; Gao, S.; Tang, W. X. *Inorg. Chem.* **2003**, *42*, 6123−6129.
(32) Li, D. F.; Gao, S.; Zheng, L. M.; Tang, W. X. *J. Chem. Soc., Dalton Trans.* **2002**, 2805−2806.
(33) Korzeniak, T.; Stadnicka, K.; Rams, M.; Sieklucka, B. *Inorg. Chem.* **2004**, *43*, 4811−4813.
(34) Lim, J. H.; You, Y. S.; Yoo, H. S.; Yoon, J. H.; Kim, J. I.; Koh, E. K.; Hong, C. S. *Inorg. Chem.* **2007**, *46*, 10578−10586.
(35) You, Y. S.; Kim, D.; Do, Y.; Oh, S. J.; Hong, C. S. *Inorg. Chem.* **2004**, *43*, 6899−6901.
(36) Kashiwagi, T.; Ohkoshi, S.; Seino, H.; Mizobe, Y.; Hashimoto, K. *J. Am. Chem. Soc.* **2004**, *126*, 5024−5025.
(37) Zhao, H. H.; Shatruk, M.; Prosvirin, A. V.; Dunbar, K. R. *Chem.—Eur. J.* **2007**, *13*, 6573−6589.
(38) Wang, Z. X.; Liu, B. L.; Wang, J.; Song, Y. *Inorg. Chem. Commun.* **2009**, *12*, 1179−1181.
(39) Venkatakrishnan, T. S.; Rajamani, R.; Ramasesha, S.; Sutter, J. P. *Inorg. Chem.* **2007**, *46*, 9569−9574.
(40) Podgajny, R.; Desplanches, C.; Sieklucka, B.; Sessoli, R.; Villar, V.; Paulsen, C.; Wernsdorfer, W.; Dromzee, Y.; Verdaguer, M. *Inorg. Chem.* **2002**, *41*, 1323−1327.
(41) Yoon, J. H.; Kim, H. C.; Hong, C. S. *Inorg. Chem.* **2005**, *44*, 7714−7716.
(42) Wang, Z. X.; Li, X. L.; Wang, T. W.; Li, Y. Z.; Ohkoshi, S.; Hashimoto, K.; Song, Y.; You, X. Z. *Inorg. Chem.* **2007**, *46*, 10990−10995.
(43) Kim, J. I.; Yoon, J. H.; Kwak, H. Y.; Koh, E. K.; Hong, C. S. *Eur. J. Inorg. Chem.* **2008**, 2756−2763.
(44) Podgajny, R.; Korzeniak, T.; Przychodzen, P.; Gimenez-Saiz, C.; Rams, M.; Kwasniak, M.; Sieklucka, B. *Eur. J. Inorg. Chem.* **2010**, 4166−4174.
(45) Wang, T. W.; Wang, J.; Ohkoshi, S.; Song, Y.; You, X. Z. *Inorg. Chem.* **2010**, *49*, 7756−7763.
(46) Song, Y.; Ohkoshi, S.; Arimoto, Y.; Seino, H.; Mizobe, Y.; Hashimoto, K. *Inorg. Chem.* **2003**, *42*, 1848−1856.
(47) Zhong, Z. J.; Seino, H.; Mizobe, Y.; Hidai, M.; Fujishima, A.; Ohkoshi, S.; Hashimoto, K. *J. Am. Chem. Soc.* **2000**, *122*, 2952−2953.
(48) Borras-Almenar, J. J.; Clemente-Juan, J. M.; Coronado, E.; Tsukerblat, B. *MAGPACK, Magnetic Properties Analysis Package for Spin Clusters*, version 00.1, 2000.
(49) Zhou, H. B.; Wang, J.; Wang, H. S.; Xu, Y. L.; Song, X. J.; Song, Y.; You, X. Z. *Inorg. Chem.* **2011**, *50*, 6868−6877.